Catalysis Today 151 (2010) 212–222

Contents lists available at ScienceDirect

Catalysis Today

journal homepage: www.elsevier.com/locate/cattod

Overview of the practically important behaviors of zeolite-based urea-SCR catalysts, using compact experimental protocol

Krishna Kamasamudram, Neal W. Currier, Xu Chen, Aleksey Yezerets*

Catalyst Technology Department, Corporate Research and Technology, Cummins Inc., 1900 McKinley Ave., Columbus, IN 47201, USA

ARTICLE INFO

Article history:
Available online 22 April 2010

Keywords:
SCR
NOx reduction
Experimental methodology
Transient performance
NO oxidation
NO_2 reduction
NH_3 oxidation
NH_3 storage
NH_4NO_3 formation
Nitrogen balance

ABSTRACT

Selective catalytic reduction with NH_3 (NH_3-SCR technology), based on $V_2O_5/WO_3/TiO_2$ catalysts, has been previously commercialized for abating NOx emissions from various stationary and mobile lean-burn or diesel engines. However, meeting the uniquely stringent US EPA 2010 regulations for diesel engines required introduction of a new class of SCR catalysts, based on Cu- or Fe-exchanged zeolites. While remarkably active and stable, these new materials proved substantially more difficult than vanadia-based catalysts to operate transiently on the road, due to their much higher NH_3 storage. The objective of this work was to develop a concise experimental protocol, elucidating multiple catalytic functions, steady-state and transient, of practical relevance to the mobile SCR applications. This paper provides a comprehensive overview of such functions, using select data from various representative Cu- and Fe-zeolite catalysts. While the bulk of the reported results originated directly from the developed protocol, additional experiments, validating the assumptions or clarifying unexpected experimental observations, are included.

1. Introduction

Despite rapid developments in the areas of alternative energy, diesel engines remain a preferred source of propulsion, especially in heavy-duty transportation. This is due to their superior fuel efficiency compared to conventional gasoline engines, high power density, and a number of other characteristics beneficial to the customer, such as high torque at low speed. However, their broader market penetration in the US has been hindered by the increasingly stringent environmental regulations, especially for the oxides of nitrogen, NO and NO_2, collectively referred to as NOx. Selective catalytic reduction with NH_3, based on $V_2O_5/WO_3/TiO_2$ catalysts, has been used for several decades to reduce NOx emissions under net oxidizing, fuel-lean conditions [1]. The same class of materials was later applied to fulfill the requirements of Euro-IV regulations for diesel-powered vehicles, using urea decomposition and hydrolysis as a source of NH_3 [2]. The more stringent US EPA 2010 on-road emission regulations, which forced catalyzed, actively regenerated diesel particulate filters (DPF) to be used along with the NOx reduction catalysts, rendered this class of catalysts impractical because they could not withstand high temperatures, in excess of 550–600 °C, associated with active DPF regeneration [3]. In response to this challenge, a number of new materials were developed in the recent years, based on mixed metal oxides, as well as Fe- and Cu-exchanged zeolites [4–9]. This latter class of catalysts possesses outstanding hydrothermal stability, as illustrated in Fig. 1.

Notwithstanding their advantageous characteristics, these zeolite-based catalysts represent both substantial new challenges and opportunities for practical application due to their much higher NH_3 storage compared to V_2O_5-based materials, as illustrated in Fig. 2. Depending on the conditions, the new zeolite catalysts may take over an hour to attain equilibrium ammonia coverage and reach steady-state performance. Thus, in real-world driving with rapidly changing temperature, flow and gas composition in the exhaust, zeolite-based SCR catalysts are operating far from steady-state most of the time. This limits the usefulness of the steady-state conversion maps such as those reported in Fig. 1. Furthermore, acting as NH_3 capacitors, the new materials drastically complicate urea dosing strategy, because at a given set of engine exhaust conditions, they behave differently depending on their ammonia coverage. Therefore, successful application of the new, zeolite-based SCR catalysts, demands detailed understanding of their performance over a broad range of conditions, including transients. In this work, an experimental protocol is defined, which was optimized to yield such information that elucidates both steady-state and transient characteristics critical to practical application.

* Corresponding author. Tel.: +1 812 377 9587.
E-mail address: aleksey.yezerets@cummins.com (A. Yezerets).

0920-5861/$ – see front matter © 2010 Elsevier B.V. All rights reserved.
doi:10.1016/j.cattod.2010.03.055

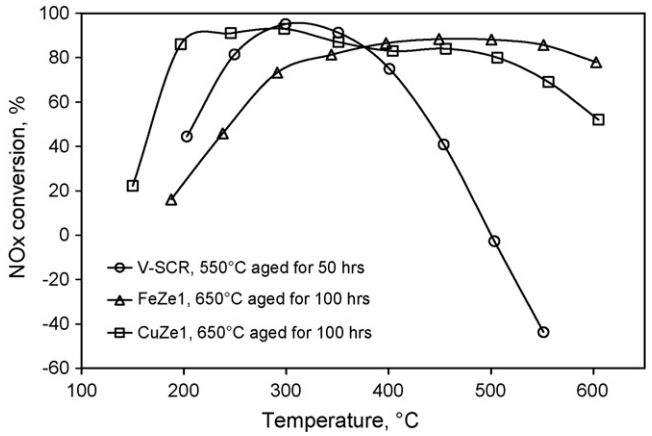

Fig. 1. Steady-state NOx conversion efficiency maps for state-of-the-art SCR catalysts, with 200 ppm NO and 200 ppm NH_3. The vanadia-based catalyst was aged at a lower temperature due to its poor hydrothermal stability, compared to the zeolite-based catalysts.

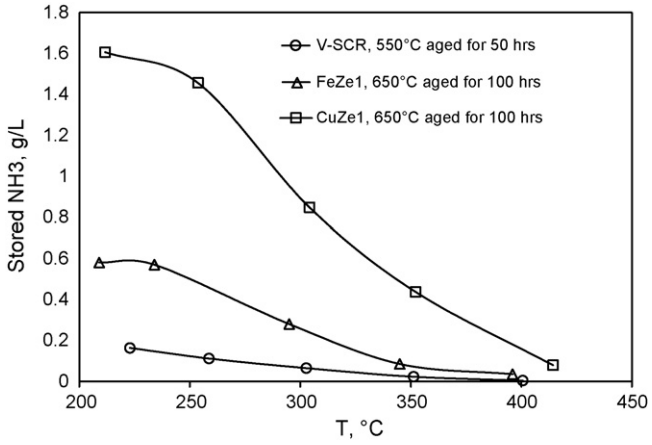

Fig. 2. Total NH_3 storage on the state-of-the-art SCR catalysts, measured with 200 ppm NH_3, 10% O_2, 8% CO_2, 7%H_2O.

2. Experimental

2.1. Bench-reactor systems

A simplified schematic of the bench-reactor system, used to collect the bulk of the data in this study, is shown in Fig. 3. The system was designed to provide rapid response to gas composition transients. To that end, the entire gas stream exiting the catalyst (typically 26 slpm) is fed directly into a fast-response model of the MKS MultiGas 2030 FTIR analyzer. Furthermore, the system can create well-defined steps in the ammonia concentration using a 4-way valve arrangement as shown in Fig. 3. A typical duration of such transition is substantially less than a second, compared to a settling time of 1–2 s when gas composition changes are achieved by commanding a mass-flow controller setting change.

The gases of research purity grade for this study were supplied by AirGas. All of the individual gases except O_2 were supplied as dilute mixtures with N_2. The precise quantity of the gases was metered using MKS mass-flow controllers. Water was introduced into the feed gas using an Isco high-pressure pump, spraying a stream of liquid onto a wick heated in excess of 200 °C. The lines in the system were heated in excess of 190 °C to prevent condensation of water or adsorption of ammonia.

A catalyst sample, with a diameter of 25.4 mm and a length of 76.2 mm (yielding GHSV of ~40k h^{-1}), was located inside a silica (fused quartz) reactor tube, which was heated using a three-zone resistance furnace from Lindberg. Using such an inert material for the reactor tube was critical to prevent undesirable reactions, such as ammonia oxidation or NO_2 reduction at high temperatures.

A reactor similar in design, but with reduced-scale, was employed to conduct several additional experiments targeted at achieving nitrogen balance. Using argon as a carrier gas and employing a SpaciMS type mass-spectrometer [10], enabled direct measurement of N_2 produced by the SCR reaction or ammonium nitrate decomposition. In order to minimize interference with N_2 measurements, because of substantial levels of CO^+, isobaric with N_2^+, in the CO_2 fragmentation pattern, CO_2 was not included in the gas stream for these experiments. The N_2 signal was calibrated using a certified gas mixture of N_2 in Ar, further diluted

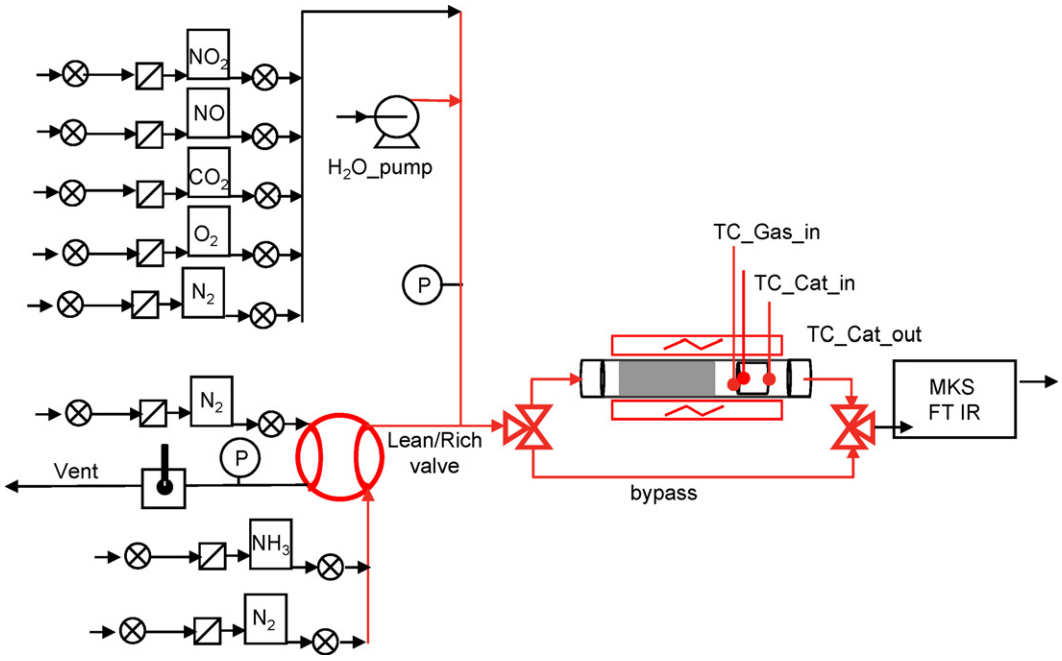

Fig. 3. Simplified schematic of the bench-reactor system.

Table 1
Catalyst samples used in this study.

Sample designation	Catalyst description	Rationale for using in this work
V-SCR	Conventional $V_2O_5/WO_3/TiO_2$ catalyst used in Euro IV applications	Representative of the current state-of-the-art for the respective classes of SCR catalysts
FeZe1	Fe-zeolite catalyst, as described in [24]	
CuZe1	Cu-zeolite catalyst, as described in [25]	
CuZe2	Experimental proprietary formulation	Less thermally stable than the state-of-the-art sample, allowing us to illustrate aging effects

by research-grade Ar to create N_2 concentrations in the range of 40–200 ppm.

2.2. Catalyst samples

All catalysts in this paper (Table 1) have been provided by Johnson Matthey. For each of the catalyst functions discussed, we chose experimental results from those samples which lent themselves to a more vivid illustration of the insights available through the developed methodology. For example, we have referred to a less stable, experimental Cu-zeolite formulation (CuZe2) to point out some of the aging effects, given that the state-of-the-art sample (CuZe1) showed minimal degradation under the aging conditions employed. All the studied catalysts were washcoated on a honeycomb cordierite substrate with a channel density of 62 cells per cm^2 (400 cells/$in.^2$).

All the catalyst samples used in this paper were subjected to some degree of hydrothermal pre-treatment under 10 vol.% O_2, 8 vol.% CO_2, 7 vol.% H_2O, balance N_2, to ensure their stable performance during the subsequent testing. The samples reported as *un-aged* have been pretreated at 600 °C for 2 h, in agreement with the "degreening" procedures commonly used in industry. The samples labeled as *aged* were exposed to the above gas mixture at 650 °C for 10 or 100 h as indicated in the text.

2.3. Experimental methodology

The experimental protocol developed includes four segments, as schematically depicted in Fig. 4. Basic components of exhaust gas (10 vol.% O_2, 8 vol.% CO_2, 7 vol.% H_2O, balance of N_2) were present during the entire experiment, while NOx and NH_3 were switched on and off, as shown. Unless indicated otherwise, the inlet concentration of both NOx and NH_3, when present, was 200 ppmv. The NO and NO_2 content of the total NOx is expressed in this paper in the form of NO_2/NOx ratio, i.e. $NO_2/(NO + NO_2)$. Duration of individual steps was varied depending on the time required to achieve steady-state.

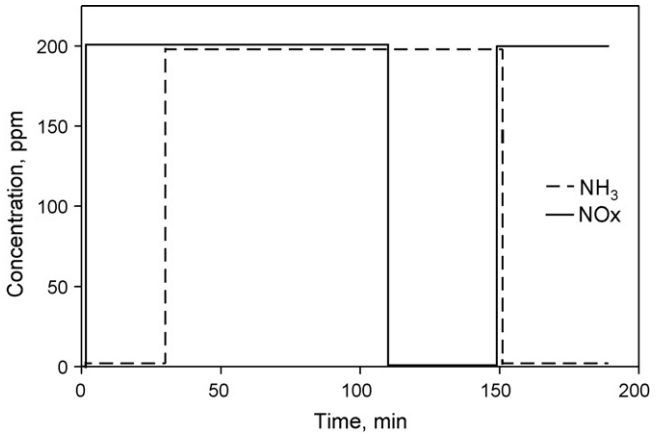

Fig. 4. Schematic representation of the 4-step experimental protocol. The lines are artificially separated for clarity.

Despite its apparent simplicity, the protocol yields information about a number of useful functions, as described in detail in the following sections. These include:

Steady-state functions:

- Step 1: $NO \leftrightarrow NO_2$ oxidation/reduction and NOx storage.
- Step 2: NOx conversion, NH_3 slip, parasitic NH_3 oxidation (as defined below), selectivity to N_2O, and the NO_2/NOx ratio at catalyst-out.
- Step 3: NH_3 oxidation by O_2 alone, including conversion and selectivity to NOx and N_2O.

Dynamic functions:

- Step 2: Equilibrium NH_3 coverage under SCR conditions, referred to as *"dynamic" capacity*, and NH_3 coverage-dependent NOx conversion.
- Step 3: Additional NH_3 storage, achievable in the absence of SCR reaction, herein referred to as *"vacant" capacity*, and a coverage-dependent NH_3 oxidation activity.
- Step 4: Equilibrium NH_3 storage capacity in the absence of SCR reaction, herein referred to as *"total" capacity*. Two independent ways of measuring the total storage capacity – directly during Step 4 and as a sum of dynamic and vacant capacities in Steps 2 and 3 – serve as an additional insurance against experimental artifacts.

This protocol was applied at a variety of experimental conditions, such as different temperatures, flow rates and gas compositions, yielding the respective parametric dependence information.

3. Experimental results

The following section contains a step-by-step review of the functions probed by the described protocol.

3.1. First step – $NO \leftrightarrow NO_2$ oxidation/reduction and storage

The NO_2/NOx ratio in zeolite-based SCR catalysts is known to have a major effect on their catalytic efficiency, with an optimum around the 0.5 value – an equimolar mixture of NO and NO_2 [11]. That is why a catalyst's ability to modify the NO_2/NOx ratio *in situ* may have a substantial impact on its performance. To individually probe the respective catalytic function, in the first step of the developed protocol, NOx is introduced alone, without NH_3.

3.1.1. NO oxidation and NO_2 reduction

An example of the $NO \leftrightarrow NO_2$ oxidation–reduction performance for a CuZe2 catalyst across the temperature range relevant to practical applications is reported in Fig. 5. As expected for a selective catalyst, it exhibited very modest oxidation activity. In the experiments with pure NO (inlet $NO_2/NOx = 0$), the rate of NO oxidation became sufficiently high, so as to allow NO_2/NOx ratio approach equilibrium, only at temperatures in excess of 500 °C. The catalyst has also exhibited poor NO_2 decomposition activity, as can be

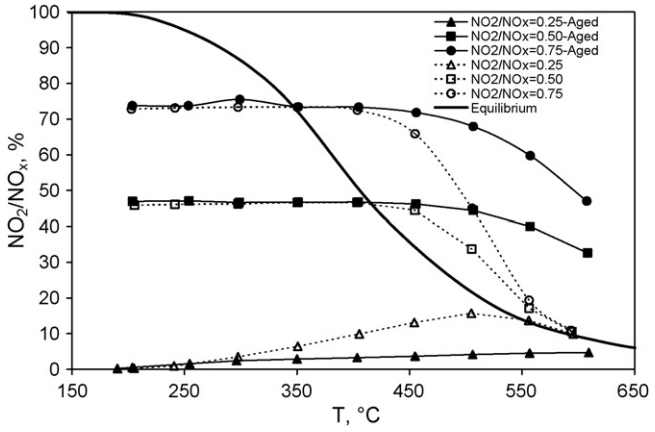

Fig. 5. Steady-state NO_2/NOx ratio at the outlet of CuZe2 catalyst, un-aged and 100-h aged. The inlet NO_2/NOx ratio values for each series are indicated on the plot.

clearly seen for the case of inlet NO_2/NOx = 0.75. The onset of NO_2 reduction could only be observed at temperatures above 450 °C; however it accelerated more rapidly with temperature than NO oxidation, hinting at higher activation energy of the former process.

The resulting data provide an opportunity to further probe these two functions, using macro-kinetic approach, to understand their nature and evaluate their change with aging. In particular, comparing apparent activation energies at the different stages of aging can yield insights into the underlying catalyst changes, the two extremes being the decrease in the number of active sites without changes to the rate-limiting step, and the change of the rate-limiting step. Therefore, the analysis was focused on deriving an apparent activation energy for catalysts at different stages of aging. This analysis was focused on the two limiting cases in our data (NO_2/NOx = 0 and 0.75) and involved only the experimental points with differential conversion and located far from equilibrium. Due to the differential conversion levels, it was possible to lump the mass-action terms into the pre-exponential factor of the Arrhenius equation, as follows:

$$r = A \times e^{(-E_a/(RT))}$$

where r is rate of NO oxidation or NO_2 reduction reaction, A is a pre-exponential factor, combining the frequency factor with the mass-action terms such as concentration of species.

The results, reported in Fig. 6 and Table 2, were consistent with the hypothesis that NO oxidation has substantially lower activation energy than NO_2 reduction. It is well known, that in the H-form, zeolites exhibit virtually no catalytic activity in the $NO \leftrightarrow NO_2$

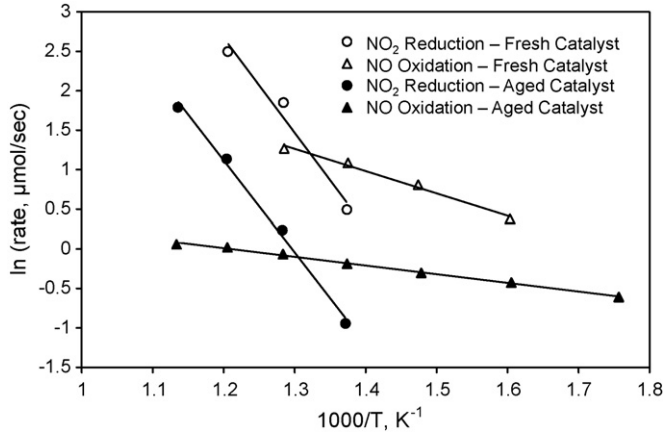

Fig. 6. Arrhenius plots based on the data from Fig. 5.

Table 2
Apparent activation energy of CuZe2 catalyst for the NO oxidation and NO_2 reduction reactions.

Sample	Activation energy, kJ/mol	
	NO oxidation	NO_2 reduction
CuZe2, un-aged	23.4 ± 1.8	99.8 ± 16.5
CuZe2, aged	9.1 ± 0.2	96.4 ± 4.8

Note: Confidence interval values are based on the standard error of slope values derived from linear regression of Arrhenius plots using Minitab 14.0 statistical software.

reactions [12]. This suggests that for Cu-exchanged zeolite, NO oxidation and NO_2 reduction reactions occur on the sites originating from the introduced metal, however with different rate-limiting steps for theses two reactions. Low activation energy of the NO oxidation process suggests that a physisorption of one of the reactants, most likely NO, serves as a rate-limiting step. On the other hand, substantially higher activation energy of the reverse reaction hints at the rate-limiting step being desorption of oxygen from the Cu–O–Cu sites [13]. It may be worth noting here that a similar clear differentiation between the activation energy of NO oxidation and NO_2 reduction was also observed in the other catalysts of this class studied to date.

Upon catalyst aging, both NO oxidation and NO_2 reduction rates have deteriorated appreciably (Fig. 5). However, the aging appears to have impacted the oxidation and reduction processes differently (Fig. 6 and Table 2). The activation energy of NO_2 reduction remained virtually unchanged. Therefore, the deterioration can be attributed to the decline in the number of active sites, without change in the rate-determining step. As an example, agglomeration of extra-framework copper oxide clusters could result in such a behavior. On the other hand, the activation energy of NO oxidation appears to have changed substantially, pointing at some changes in the active site or in the rate-determining step.

The data in Fig. 5 also provide anecdotal indication that NO_2 may be inhibiting the forward reaction. In the case of pure NO (NO_2/NOx = 0), measurable conversion of NO to NO_2 is observed at 350 °C, substantially beyond experimental uncertainty. However, at the same temperature and at NO_2/NOx = 0.5 we detected no measurable conversion of NO, even though such conversion would be thermodynamically favorable. It should be noted, that NO_2 inhibition, if confirmed, should be accounted for in the rate constant calculations, likely resulting in an effective increase in the apparent activation energy, e.g. as described by Mulla et al. [14].

3.1.2. NOx storage

In addition to the $NO \leftrightarrow NO_2$ oxidation/reduction behavior, the first step of the protocol, in principle, measures NOx storage on the SCR catalyst by integrating the difference between the inlet and outlet NOx concentration profiles upon a step change in NOx concentration. However, for all the studied catalysts, virtually no NOx storage was observed under the experimental conditions described. Due to the rapid response capabilities of the employed bench reactor, NOx storage could be detected and quantified at the levels substantially below ~1 μmol of NOx for a fully formulated, washcoated catalyst sample weighing ~15–20 g. Using the units commonly accepted in the industry for expressing storage on the monolith-supported catalysts, this is equivalent to ~1 mg NOx per liter of the catalyst. By comparison, as illustrated in Fig. 2, the amount of ammonia stored on the catalyst was in the range of several gNH_3/l catalyst, i.e. three to four orders of magnitude higher.

Lack of measurable NOx storage was surprising in the light of abundant spectroscopic evidence of NOx being adsorbed on the surface of the zeolite-based SCR catalyst as nitrates or nitrites [15,16]. One of the possible explanations for this apparent con-

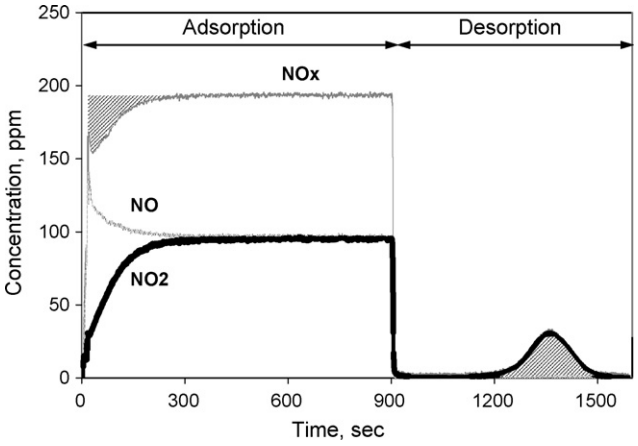

Fig. 7. NOx adsorption/desorption experiment with FeZe1, un-aged. The adsorption segment was conducted at 190 °C, with 100 ppm NO, 100 ppm NO_2, 10% O_2, and 8% CO_2 in the gas feed. During the TPD segment, the temperature was ramped up at 10 °C/min, with only the balance gas (N_2) present in the gas feed.

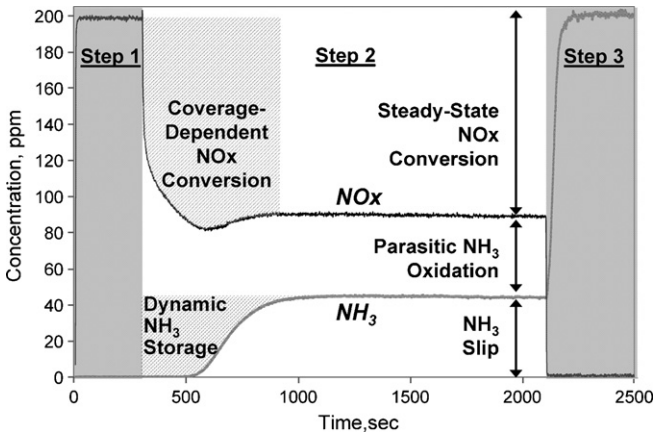

Fig. 9. Example of the outlet gas traces during the second step of the experimental protocol. FeZe1 catalyst aged for 50 h; reaction temperature 240 °C; gas feed includes 200 ppm NO, 200 ppm NH_3.

tradiction is due to the absence of water vapor in the typical *in situ* IR experiments. To verify this hypothesis, a set of additional NOx adsorption–desorption experiments, in the presence and in the absence of water vapor in the gas feed, was conducted. After 15 min of saturation exposure, NOx was switched off and the temperature was ramped to 500 °C at the rate of 10 °C/min. As shown in Fig. 7, substantial storage and release of NOx were observed in the absence of water. In all of such experiments, the integral amounts of NOx stored and released, illustrated by the shaded areas on the plot, were similar within 3%. In the example reported in Fig. 7, the inlet NO_2/NOx ratio was 0.5. During the early stages of the storage process, NO_2 was being disproportionately consumed, while additional NO was released. The ratio of the integrated amounts of disappeared NO_2 and produced NO was close to 3, suggesting that NO_2 storage was occurring via a disproportionation mechanism, resulting in two NO_2 molecules oxidized and adsorbed as nitrates due to the third one being reduced to NO. Also, during the temperature-programmed desorption (TPD) step, NO_2 was essentially the only NOx species present among the desorption products, consistent with decomposition of the stored nitrate species.

However, when a similar experiment was conducted in the presence of water, no storage or release of NOx was detected within the experimental uncertainty. Fig. 8 compares TPD steps in the

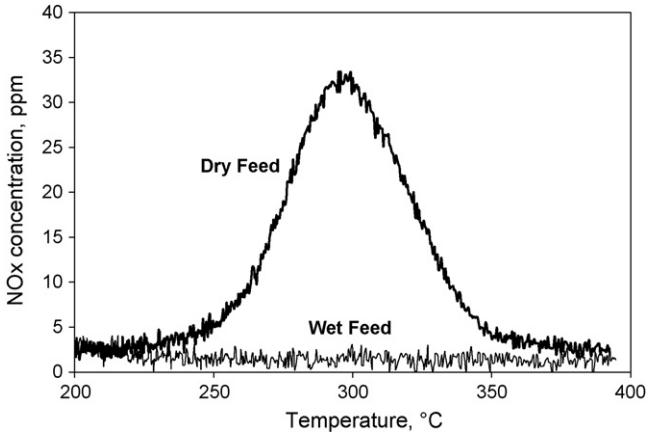

Fig. 8. NOx desorption profiled during a TPD, following NOx storage at 190 °C. The catalyst sample and conditions are identical to those in Fig. 7, except that 7% H_2O water vapor was used during NOx storage exposure in the experiment labeled as "wet feed".

presence and in the absence of water. Therefore, dry conditions indeed exaggerate NOx storage on this class of catalysts, arguably because water effectively competes with NOx for adsorption sites [17].

These results should not be interpreted as a proof that NOx is not adsorbed at all on the catalyst surface under the practically relevant, wet conditions. In particular, they do not indicate that the SCR reaction is proceeding via the Eley-Rideal mechanism, with NH_3 adsorbed on the surface, and NOx reacting directly from the gas phase. They merely imply that the amount of NOx stored on the catalyst is very small and inconsequential for its transient behavior. In other words, for the purposes of practical application of these catalysts, NO ↔ NO_2 processes can be treated as steady-state.

3.2. Second step – SCR reaction

The second step in the developed protocol is focused on characterizing the target function – SCR performance. At the beginning of this step NH_3 is introduced via a step change, with NOx being already present in the gas feed. An example of catalyst behavior during Step 2 is shown in Fig. 9. Upon introduction of ammonia, NOx concentration starts declining, but rather slowly due to a concurrent process of NH_3 storage. With progressive saturation of the surface, NOx concentration at the catalyst outlet may decline monotonically, or pass through a minimum, as can be seen around 600 s in Fig. 9. Once NH_3 storage is saturated, the process arrives at steady-state, yielding such commonly reported characteristics as steady-state NOx conversion and NH_3 slip, as well as selectivity to N_2O and NO_2/NOx ratio in the reaction products. The instantaneous imbalance between disappearing NOx and NH_3, clearly observable under steady-state conditions, is attributed to the oxidation of NH_3 by oxygen to produce N_2. We refer to this undesirable, non-selective process as *parasitic NH_3 oxidation*, since it consumes the valuable reductant.

3.2.1. Steady-state NOx conversion and NH_3 slip

Fig. 10 shows an example of steady-state SCR conversion and NH_3 slip, reported against stoichiometric *ammonia/NOx molar ratio* (*ANR*). As expected, at low ANR values, NOx conversion responded nearly stoichiometrically to the ANR, implying that when ammonia is in deficit, it gets utilized very selectively across this broad range of temperatures. However, as ANR approaches unity, differences in behavior depending on the temperature become obvious. At the highest temperatures (e.g., 600 °C), a substantial amount of ammonia is consumed parasitically. As a result, injecting over-stoichiometric amounts of NH_3 (ANR > 1) leads to improved NOx

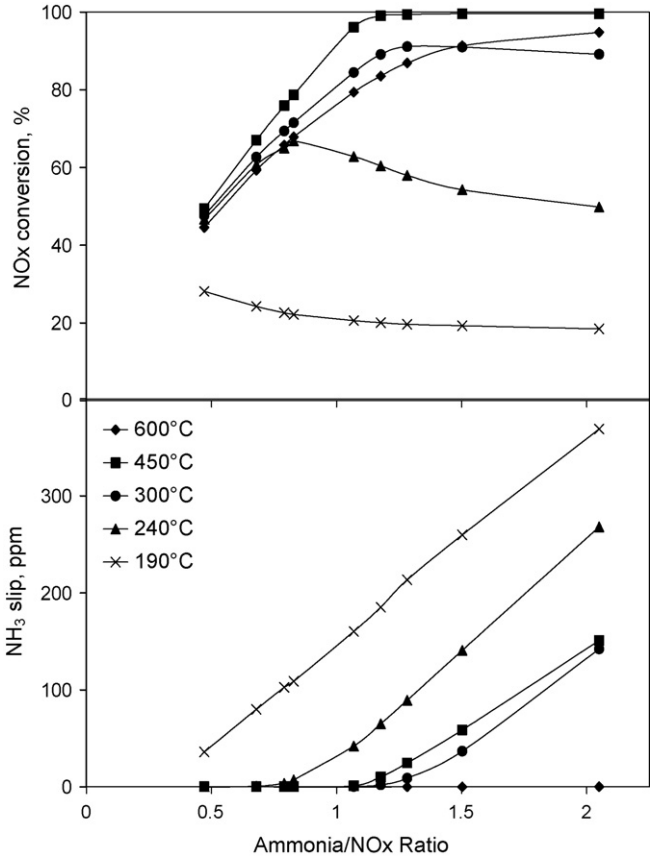

Fig. 10. Impact of ANR on steady-state NOx conversion and NH_3 slip for un-aged FeZe1 catalyst; gas feed includes 200 ppm NO and variable amounts of NH_3, as per ANR values indicated in the legend.

conversion, with negligible NH_3 slip. In the intermediate temperature range, conditions close to optimal for this catalyst, nearly complete conversion can be achieved around the stoichiometric point. Excessive amounts of introduced ammonia mostly lead to an increased NH_3 slip, caused by catalyst's limited NH_3 oxidation activity in this temperature range. At the lowest temperatures, a more complex performance is observed. For example, at 240 °C, maximum steady-state NOx conversion was observed around ANR of 0.8. Further increase in the ANR lead to a nearly quantitative slip of ammonia, and inhibited the rate of SCR reaction, as further briefly discussed below.

Another example of the steady-state NOx conversion results is reported in Fig. 11, representing the effect of NOx concentration on the SCR efficiency, at ANR = 1. In other words, concentrations of NOx and NH_3 were varied in unison. For the sake of presentation clarity, we are only reporting the results obtained at the highest and lowest studied temperatures. At the low temperature, NOx conversion was virtually unaffected by the NOx and NH_3 concentrations. This implies that the rate of reaction was growing nearly linearly. On the other hand, under the high-temperature conditions, NOx conversion was accelerating with the increased concentrations of NOx and NH_3. The latter was reflected in a faster than linear (but slower than quadratic) increase in the reaction rate. These results are consistent, for example, with the kinetic formalism proposed by Masaoki et al. [18] and Olsson et al. [19], where at low temperatures the overall SCR reaction has first order with respect to NO and pseudo-zero order with respect to NH_3, due to its strong chemisorption. As ammonia adsorption weakens with temperature, the respective reaction order departs from zero and becomes a positive fractional value.

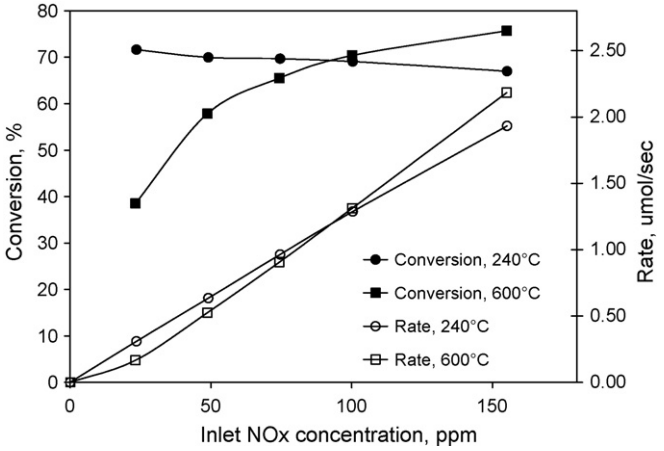

Fig. 11. Impact of NOx concentration, at ANR = 1, on NOx reduction over un-aged FeZe1 catalyst, at the low- and high-temperature boundaries of the practically relevant temperature range.

3.2.2. *Steady-state parasitic NH_3 oxidation*

As mentioned in Section 3.2, the instantaneous imbalance between the amounts of NOx and NH_3 consumed is commonly attributed to a parasitic oxidation of the latter, yielding N_2. That imbalance is most obvious at steady-state conditions, when NH_3 storage is saturated and NH_3 disappearance should only be due to its oxidation. There is no doubt that the parasitic oxidation also occurs during the approach to steady-state, however this would be impossible to decouple from the storage without directly measuring the product of the oxidation reaction – N_2.

In order to address this experimental difficulty, we have conducted a separate set of experiments using a different bench-reactor system, dedicated to measuring N_2. As described in Section 2, this system employs argon as a balance gas and a mass-spectrometer in order to measure N_2 produced in the reaction. The results reported in Fig. 12 show that the amount of N_2 inferred from the other N-species, measured by FTIR was in excellent agreement with the amount of N_2 directly detected by mass-spectrometer. This finding supports the above assumption that NH_3 disappearance for reasons other than reaction with NOx or storage, can be attributed to its parasitic oxidation.

Being a product of competition between NH_3 reactions with NOx and oxygen, parasitic NH_3 oxidation exhibits complex dependencies on the process parameters, such as temperature and

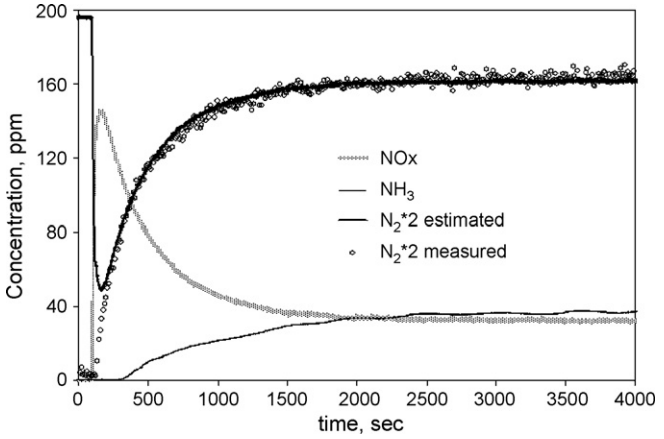

Fig. 12. Nitrogen balance verification for un-aged CuZe1 catalyst, with gas feed containing 200 ppm NO and 200 ppm NH_3, at 250 °C. Concentrations of NO, NO_2 NH_3 and N_2O (not reported – virtually absent in this experiment) were measured using FTIR; concentration of N_2 – using mass-spectrometer.

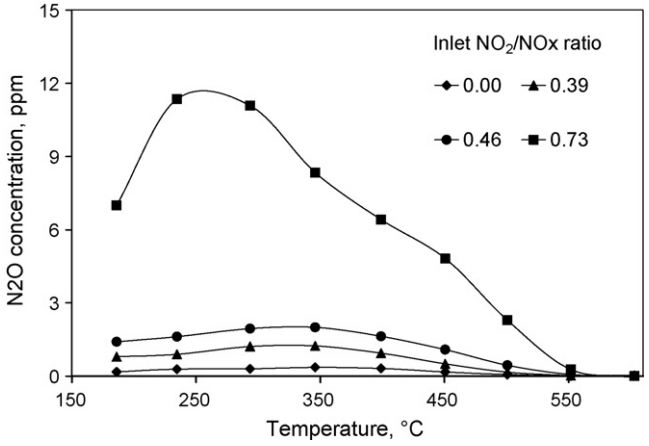

Fig. 13. Impact of NO_2/NOx ratio on N_2O yeild from un-aged FeZe1 catalyst.

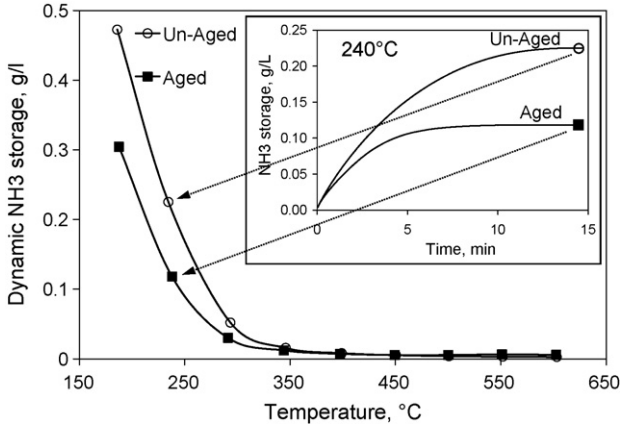

Fig. 14. Dynamic NH_3 storage on FeZe1, un-aged and 100-h aged.

concentration. An example of that behavior is discussed in Section 3.3.1.

3.2.3. Selectivity to N_2O, NO, NO_2

Two other features which can be measured during the second step of the protocol are related to the SCR reaction selectivity to N_2O, as well as the NO_2/NOx ratio at the catalyst outlet. The latter can provide some interesting transient insights, for example related to the change in the oxidation state of the active site in the presence of NOx, especially NO_2; however at steady-state conditions, the ratio appears to merely follow the intuitive direction. Depending on the inlet NO_2/NOx ratio, the catalyst preferentially consumes the NOx specie present in abundance. Therefore, the outlet NO_2/NOx ratio is typically shifted towards the equimolar mixture.

On the other hand, N_2O traces can yield useful information about the reaction mechanism. According to the [20], formation of N_2O is inherent to the nitrate decomposition branch of the reaction pathway. In accord with their findings, we invariably observe that N_2O formation is favored by the NO_2/NOx ratios above equimolar, and by lower temperatures, as shown in Fig. 13.

3.2.4. NH_3 storage under the SCR conditions

During the second step of the protocol, we can track the instantaneous amount of ammonia stored on the catalyst surface by integrating the disappearance of NH_3 and subtracting the amount of ammonia parasitically oxidized. Such attribution of missing ammonia is justified based on the nitrogen balance experiments, as the one described in Section 3.2.2.

The inset in Fig. 14 shows an example of NH_3 coverage plots thus derived. The final, equilibrium values of NH_3 coverage under SCR reaction conditions at various temperatures are reported in the main panel of Fig. 14. As will be discussed below, such dynamic ammonia storage values represent a fraction of the total amount of ammonia which can be stored on the catalyst at a given set of conditions, due to SCR reaction competing with the storage process.

3.2.5. Coverage-dependent NOx conversion

Due to the ability to track the ammonia coverage, the second step of the experimental protocol yields information about coverage-dependent NOx conversion, from the ammonia-free surface, up to the dynamic coverage value. The example presented in Fig. 15 was chosen to illustrate that in some cases, most notably on Fe-zeolite catalysts, maximum NOx conversion is achieved at some intermediate level of ammonia coverage. The same effect is reflected in the steady-state conversion dependence on ammonia concentration at low temperatures, as shown in Fig. 10. Such volcano dependence is often attributed to the inhibition of the reaction rate at high levels of ammonia coverage [21,22]. The practical implication of this behavior is that the urea dosing control must be targeting not a maximum, but some intermediate optimum level of coverage, a very difficult task in the real-world operation.

The example presented in Fig. 15 further illustrates that this behavior can be affected by the catalyst age. With progressive aging of the FeZe1 catalyst, its dynamic ammonia storage at the reported conditions was reduced, and the inhibition effect became more pronounced.

It is worth noting that similar apparent phenomenology can be caused by a different factor under some specific conditions. In particular, a combination of low temperatures and high NO_2/NOx ratios can cause slow deactivation of the SCR reaction due to the formation of ammonium nitrate on the catalyst surface [23]. Unlike the ammonia coverage inhibition, this process is not specific to Fe-zeolite catalysts only, and can occur on Cu-zeolites as well, as indicated in Fig. 16. In this experiment, conducted using the bench reactor capable of direct N_2 measurements, the formation of NH_4NO_3 was evidenced by the instantaneous nitrogen imbalance based on the gaseous products. During the subsequent TPD, ammonium nitrate decomposed, producing comparable quantities of N_2O and N_2. The integral amounts of NOx disappearing during the storage and evolving during the TPD were balanced in our experiments within 10%. Nitrogen imbalance during SCR reaction, as well as evolution of N_2O and N_2 during subsequent TPD, were only pronounced at conditions conducive to the formation of ammonium nitrate, such as temperatures below ~250 °C and over-equimolar ratios of NO_2 and NO.

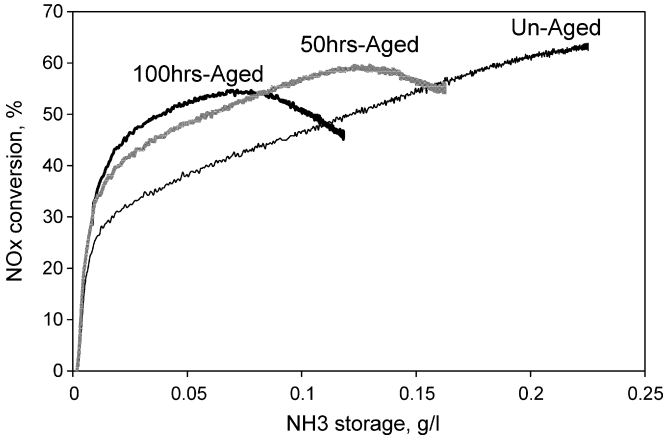

Fig. 15. Coverage-dependence of NH_3 conversion over FeZe1 at 235 °C.

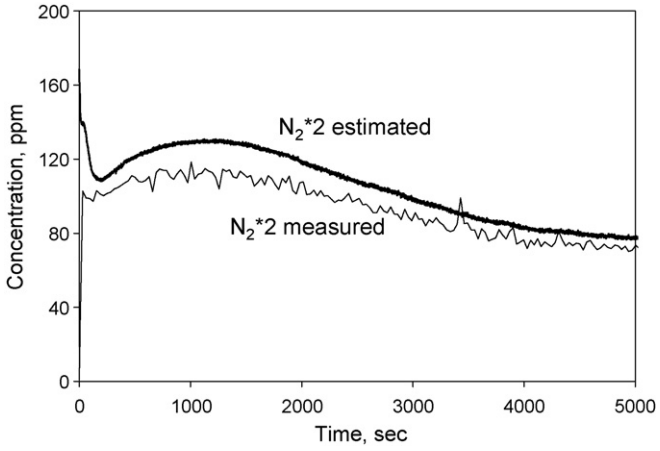

Fig. 16. Evidence of NH_4NO_3 formation over CuZe1, based on instantaneous N-imbalance during SCR reaction. Gas feed contained 50 ppm NO, 150 ppm NO_2 and 200 ppm NH_3, at 200 °C. Estimated N_2 concentration was derived from the FTIR measurements as follows: $NOx_{(in)}$–$NOx_{(out)}$–$N_2O_{(out)}$. Concentration of N_2 was measured using mass-spectrometer.

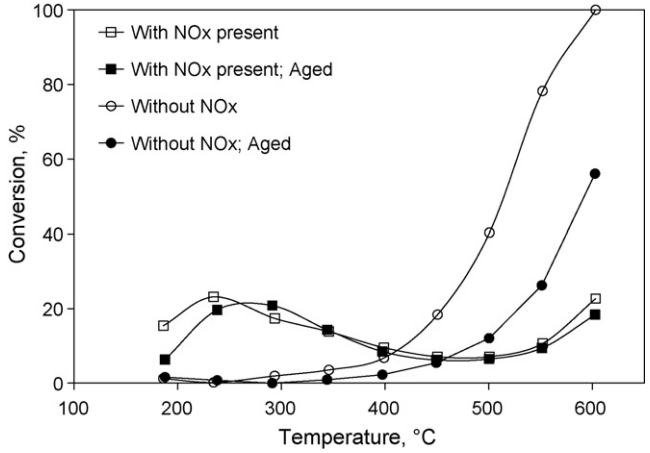

Fig. 18. Oxidation of ammonia (200 ppm) over FeZe1 (un-aged and 100 h aged), with and without NOx in the gas feed. In the experiments with NOx, feed gas included 200 ppm NO.

Overall, the second step of the developed protocol provides the bulk of the information about the SCR reaction as such, while the other steps supplement it with additional characterization of some key contributing catalytic functions.

3.3. Third step – NH_3 oxidation and additional storage

During the third step of the experimental protocol, ammonia alone is present in the gas feed, without NOx, in accordance with Fig. 4. This allows us to estimate additional amount of ammonia which can get stored on the catalyst, once SCR reaction is no longer consuming some of the stored NH_3. This step further allows us to quantify steady-state ammonia oxidation by oxygen alone, in the absence of NOx. That process can, in principle, produce other species than N_2, such as NOx or N_2O. However, in practice, today's state-of-the-art SCR catalysts exhibit a nearly quantitative selectivity to N_2 when oxidizing ammonia even at high temperatures. An example of gas concentration profiles during the third step is presented in Fig. 17.

3.3.1. NH_3 oxidation by oxygen

Fig. 18 compares ammonia conversion by oxygen in the presence and in the absence of NOx; the former values are derived during Step 2 as described in Section 3.2.2; the latter, during Step 3.

In the absence of NOx (lines with circle markers in Fig. 18), ammonia oxidation reaction lends itself to a straightforward quantitative characterization and macro-kinetic analysis, similar to the approach described in Section 3.1.1. However, since this set of experiments spanned a range of NH_3 concentrations, it was important first to determine the reaction order with regards to ammonia, to pave the way for the determination of the apparent activation energy.

$$r = [NH_3]^n A \times e^{(-E_a/(RT))}$$

where r is rate of NH_3 oxidation, A is a pre-exponential factor, combining the frequency factor with the mass-action term related to oxygen concentration $[NH_3]$ is concentration of ammonia n is reaction order with respect to ammonia.

As shown in Figs. 19 and 20 and Table 3, the process can be well fitted, over a broad range of experimental conditions, using a fractional positive reaction order in ammonia of 0.77 ± 0.02 and an activation energy of 68.7 ± 6.3 kJ/mol. It may be interesting to note here, that the activation energy is statistically different from the values reported above for both NO oxidation and NO_2 reduction, suggesting that all three red-ox processes have different rate-determining steps. Another remarkable observation is that the fractional order is maintained across a broad range of temper-

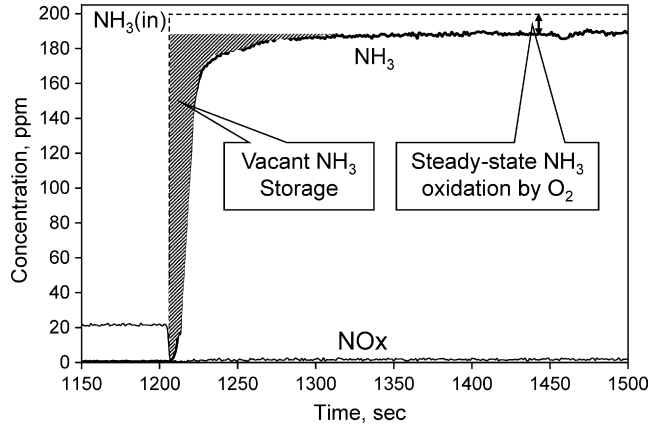

Fig. 17. Example of the outlet gas traces during the third step of the experimental protocol. FeZe1 catalyst aged for 50 h; reaction temperature 400 °C; gas feed includes 200 ppm NO, 200 ppm NH_3.

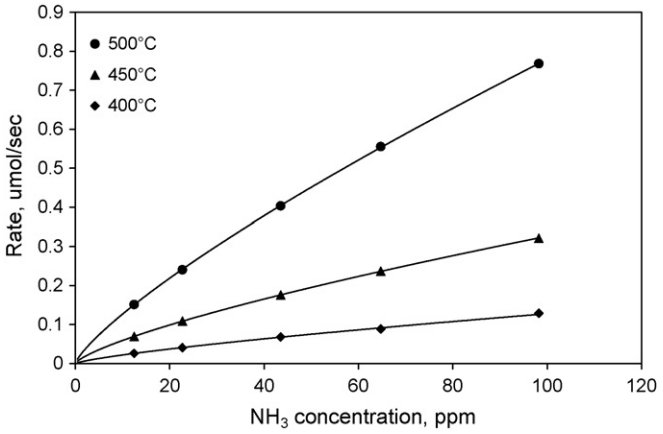

Fig. 19. Impact of ammonia concentration on its oxidation by oxygen over un-aged FeZe1 at the indicated temperatures.

Table 3
Kinetic parameters of ammonia oxidation by oxygen over un-aged FeZe1 catalyst.

	Temperature, °C			Mean	Standard deviation
	400	450	500		
Reaction order	0.77	0.74	0.79	0.77	0.02

	NH_3 concentration, ppm					Mean	Standard deviation
	98	65	44	23	12		
Activation energy, kJ/mol	78.5	71.5	63.5	65.3	64.6	68.7	6.3

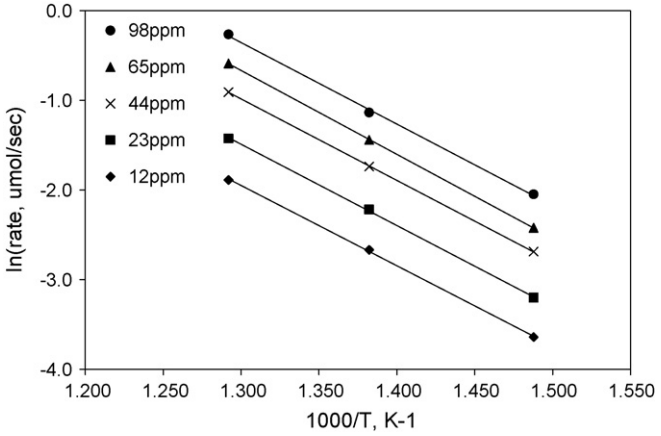

Fig. 20. Impact of temperature on ammonia oxidation at various concentrations, over un-aged FeZe1.

atures (100 °C), suggesting that it is not caused by a mixed kinetic control.

On the other hand, parasitic ammonia oxidation (lines with square markers in Fig. 18), exhibit a more complex behavior for FeZe1 catalyst. At lower temperatures, while $NH_3 + O_2$ reaction is not pronounced yet, some parasitic ammonia oxidation is already apparent in the presence of NOx. This means that limited amounts of ammonia at those conditions are oxidized by NOx without reducing the latter to N_2 or N_2O. This is likely to occur via a reaction of NH_3 either with the *in situ* produced NO_2, or with a surface site oxidized by the NO_2. In both cases, NO_2 can be reduced to NO. This process occurs in parallel with the target SCR reaction (reducing NOx to N_2) and only accounts for a limited loss of the NH_3 utilization selectivity at low temperatures. In the intermediate temperature range, parasitic oxidation declines, evidently because the accelerating SCR reaction competes more effectively with the above parasitic reaction. Finally, at higher temperatures, parasitic oxidation by oxygen starts competing noticeably with the SCR reaction. It should also be noted that, in principle, formation of ammonium nitrate, as described in Section 3.2.5, could, have further contributed to such a complex behavior, however we believe that it played no role in the specific reported experiments since its formation typically required high NO_2/NOx ratios. To summarize, we believe that a complex profile of parasitic ammonia oxidation presented in Fig. 18 can be explained due to a competition between ammonia oxidation by NO_2 or by an oxidized site produced by reaction with NO_2 (whereby the latter is only reduced to NO), by oxygen, and the SCR reaction as such, between NOx and NH_3 leading to N_2.

It is interesting to note, that FeZe1 catalyst aging has substantially reduced its activity in the $NH_3 + O_2$ process, in accord with a loss of other red-ox functions, such as NO oxidation and NO_2 reduction, as discussed above. Remarkably, parasitic ammonia oxidation remained virtually unchanged upon aging.

3.3.2. *Vacant ammonia storage*

As defined in Section 2.3, *vacant storage* represents the difference between the amount of ammonia stored on the catalyst under the steady-state SCR conditions, and the maximum amount the catalyst can store at this temperature and ammonia concentration. The difference is due to stored NH_3 being continuously consumed by reacting with NOx and O_2. We can directly estimate this vacant ammonia storage by integrating the additional uptake in Step 3, as shown in Fig. 17. Higher SCR reaction rate resulted in a larger percentage of the total storage remaining vacant. This effect is illustrated in Fig. 21, which compares experiments with NO_2/NOx ratios of 0 and 0.5. The filled part of the bars represents the dynamic ammonia coverage, measured during the second step of the protocol, i.e. under the SCR reaction conditions. The empty part of the bar corresponds to the vacant capacity measured during Step 3, i.e. in the absence of reaction with NOx. The total height of the bar is a sum of the dynamic and vacant storage and reflects the total capacity at a given temperature and NH_3 concentration of 200 ppm. The rate of reaction is faster at the optimum NO_2/NOx ratio of 0.5, compared to the "slow" SCR at NO_2/NOx = 0, and so the larger percentage of the capacity remains vacant under the SCR conditions. Similarly, as the rate of NH_3 reactions accelerates with tempera-

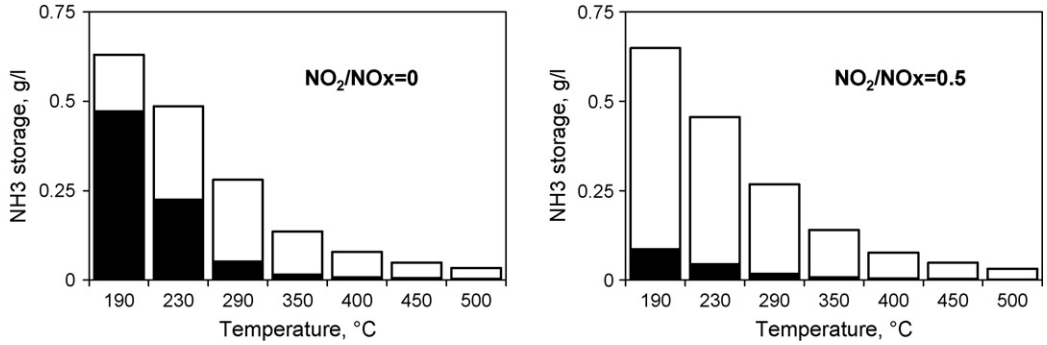

Fig. 21. Ammonia storage capacity of un-aged FeZe1. The filled part of the bar represents dynamic capacity, the empty part – vacant capacity; total height of the bar – total capacity.

ture, the larger and larger percentage of the total capacity remains vacant.

One practical implication is that only a fraction of the total capacity is occupied under the normal operating conditions, which somewhat diminishes the challenge of operating these ammonia "capacitors", as described in the introduction. On the other hand, it is clear that maps of the total ammonia storage capacity, easily obtainable in the lab (e.g., as shown in Fig. 2), are inadequate for controlling the SCR system, since the actual coverage can be drastically different depending on the rate of reactions consuming ammonia.

3.4. Fourth step – NOx reaction with NH_3-saturated surface

At the beginning of the fourth step of the developed protocol, catalyst surface is saturated with ammonia, at the level dictated by the adsorption–desorption equilibrium for the given temperature and partial pressure of ammonia. Switching off NH_3 and re-introducing NOx allows us to perform several measurements, complementary to those derived in steps two and three of the protocol, as follows.

3.4.1. Direct measurements of the total ammonia storage

Integrating the amount of NOx consumed by reacting with the stored ammonia, along with the ammonia desorbed from the catalyst, yields the direct estimation of the total ammonia storage capacity. This value is redundant to the sum of dynamic and vacant capacities, derived during steps two and three. Indeed, in our experiments we find that these ammonia storage measurements (from Step 4 and from Steps 2 + 3) usually agree quite well, serving as an additional evidence of data integrity.

3.4.2. Coverage-dependence of NOx conversion during surface NH_3 depletion

The final step of the protocol provides a somewhat different insight into the coverage-dependent NOx conversion than the second step. In the latter case, we start with the ammonia-free surface, and arrive to the "dynamic" saturation level. Also, during that second step, NH_3 is present both on the surface and in the gas phase. Finally, the observed NOx behavior can be affected by other phenomena possible when both NOx and NH_3 are fed into the catalyst, such as accumulation of ammonium nitrate, as discussed in Section 3.2.5. However, in the fourth step, we start with the surface saturated by ammonia ("total" capacity), and virtually no ammonia is present in the gas phase.

Fig. 22 provides an example of coverage-dependent NOx conversion from the second and fourth steps. The arrows represent the direction of the process, from NH_3-free to dynamic storage level for Step 2 and from the total storage level to NH_3-free surface for Step 4. At the same level of surface coverage, the rate of reaction during Step 2 was higher, arguably due to ammonia present in the gas phase. A hypothesis explaining this observation is that the sites responsible for the bulk of ammonia storage represent merely a spectator reservoir, while the sites involved in the rate-determining step of the SCR reaction contribute very little to the total storage. The latter sites could be, for example, represented by the exchanged metal ions, the former – by Brönsted acid sites. With no ammonia in the gas phase, the rate-limiting step is migration of NH_3 from the spectator sites to the active ones. On the other hand, with ammonia present in the gas feed, higher coverage of the catalytically active sites could be realized at the same level of ammonia stored in the reservoir, leading to a higher overall reaction rate. The reported data are insufficient to corroborate this hypothesis.

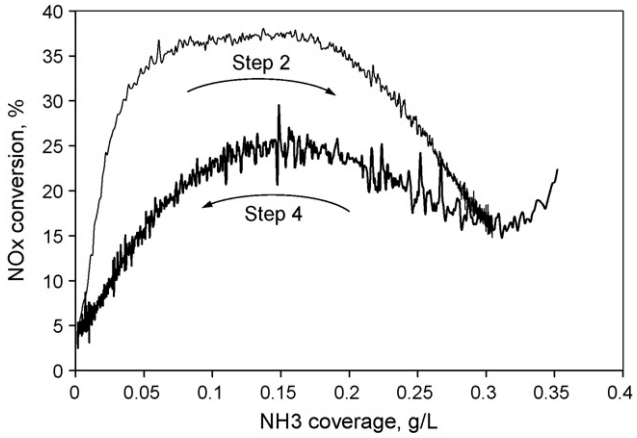

Fig. 22. Coverage-dependent NOx conversion, derived during second and fourth steps of the experimental protocol. 100 h aged FeZe1 catalyst was used in this test, with the reaction temperature of 190 °C and gas feed containing 200 ppm NO and 200 ppm NH_3.

3.4.3. Establishing NH_3-free surface

Finally, the last step of the experimental protocol serves a convenient logistical function, by cleaning the surface from ammonia and thus establishing the required, NH_3-free initial surface state for the subsequent experimental points. This obviates the need in heating up the catalyst to desorb ammonia, a step which often takes a long time with a conventional bench-reactor design.

4. Summary

The information obtained through the developed protocol can guide the design and development of SCR system as well as optimization of the urea dosing control through function-specific process understanding.

At the stage of the catalyst system design, the choice of the catalyst formulation and catalytic device sizing are both highly dependent on matching catalyst properties to the application. For example, applications with very pronounced temperature transients in the low-temperature range, such as urban stop-and-go cycles, could benefit from catalysts with reduced ammonia "capacitor". For such a catalyst, less time to achieve higher levels of ammonia coverage is required for good NOx conversion. Also, with less storage, less ammonia would get desorbed from the SCR catalyst upon a high-temperature excursion. That, in turn, should alleviate the need for treating ammonia slip. Also, using coverage-dependent NOx conversions, instead of the typical steady-state conversion maps, leads to a more accurate representation of the catalyst capabilities under a real-world driving cycle.

Function-specific catalyst understanding is also critical for optimizing the amount of urea injected into exhaust. For example, the coverage-dependent reaction rate characteristics affect the desired dosing levels in order to target either some optimal intermediate level of storage for the catalysts showing ammonia inhibition, or the maximum possible coverage for the catalysts with no inhibition. Also, quantitative understanding of the ammonia storage, and especially the distinction between the dynamic and total NH_3 capacity, enables more accurate targeting of the coverage for optimal SCR performance. Furthermore, the catalysts' activity and selectivity in oxidizing ammonia by oxygen are the key limiting factors for the maximum urea dosing rates at higher temperatures.

The developed protocol further provides insights into function-specific aging of SCR catalysts to accurately represent catalyst aging in laboratory experiments, size the system properly for the end of

useful life, and adjust urea dosing to the evolution of catalyst properties. For example, the three red-ox processes discussed above (NH_3 oxidation, NO oxidation and NO_2 reduction) appear to have different rate-determining steps and as a result, change differently with aging, while likely all occurring on the metal sites. As a result, catalyst sensitivity to the inlet NO_2/NOx ratio and ammonia/NOx ratio can follow different aging trajectories.

Finally, the quantified catalysts' selectivity to such by-products as N_2O and NH_4NO_3 allows their minimization to be included among the key criteria for the overall system and dosing control optimization.

Acknowledgements

The authors express sincere gratitude to Dr. Haiying Chen, Dr. Joseph Fedeyko, and Dr. Mario Castagnola of Johnson Matthey, for providing catalyst samples and, in particular, for very valuable discussions.

We would also like to thank Mr. Randall P. Jines and Mr. Jason L. Ferguson for their help with collecting experimental data.

References

[1] P. Forzatti, Appl. Catal. A 222 (2001) 221.
[2] I. Gekas, A. Vressner, K. Johansen, SAE 2009-01-0626.
[3] G. Cavataio, J. Girard, J.E. Patterson, C. Montreuil, Y. Cheng, C.K. Lambert, SAE 2007-01-1575.
[4] M. Schwidder, S. Heikens, A. De Toni, S. Geisler, M. Berndt, A. Brückner, W. Grünert, J. Catal. 259 (2008) 96.
[5] R.Q. Long, R.T. Yang, J. Am. Chem. Soc. 121 (1999) 5595.
[6] H.Y. Chen, W.M.H. Sachtler, Catal. Today 42 (1998) 73.
[7] P. Balle, B. Geiger, D. Klukowski, M. Pignatelli, S. Wohnrau, M. Menzel, I. Zirkwa, G. Brunklaus, S. Kureti, Appl. Catal. B 91 (2009) 587.
[8] S. Verdier, E. Rohart, H. Bradshaw, D. Harris, Ph. Bichon, G. Delahay, SAE 2008-01-1022.
[9] G. Cavataio, H.-W. Jen, J.R. Warner, J.W. Girard, J.Y. Kim, C.K. Lambert, SAE 2008-01-1025.
[10] W.P. Partridge, J.-S. Choi, Appl. Catal. B 91 (2009) 144.
[11] A. Grossale, I. Nova, E. Tronconi, D. Chatterjee, M. Weibel, J. Catal. 256 (2008) 312.
[12] M. Devadas, O. Krocher, M. Elsener, A. Wokaun, G. Mitrikas, N. Soger, M. Pfeifer, Y. Demel, L. Mussmann, Catal. Today 119 (2007) 134.
[13] B.R. Wood, J.A. Reimer, A.T. Bell, M.T. Janicke, K.C. Ott, J. Catal. 224 (2004) 148.
[14] S.S. Mulla, N. Chen, L. Cumaranatunge, G.E. Blau, D.Y. Zemlyanov, W.N. Delgass, W.S. Epling, F.H. Ribeiro, J. Catal. 241 (2006) 389.
[15] M. Iwasaki, K. Yamazaki, K. Banno, H. Shinjoh, J. Catal. 260 (2008) 205.
[16] L. Olsson, H. Sjovall, R.J. Blint, Appl. Catal. B 87 (2009) 200.
[17] R. Brosius, D. Habermacher, J.A. Martens, L. Vradman, M. Herskowitz, L. Capek, Z. Sobalık, J. Dedecek, B. Wichterlova, V. Tokarova, O. Gonsiorova, Top. Catal. 30/31 (2004) 333.
[18] M. Iwasaki, K. Yamazaki, H. Shinjoh, Appl. Catal. A 366 (2009) 84.
[19] L. Olsson, H. Sjovall, R.J. Blint, Appl. Catal. B 81 (2008) 203.
[20] M. Koebel, G. Madia, M. Elsener, Catal. Today 73 (2002) 239.
[21] A. Grossale, I. Nova, E. Tronconi, Catal. Today 136 (2008) 18.
[22] O. Krocher, Stud. Surf. Sci. Catal. 171 (2007) 261.
[23] A. Grossale, I. Nova, E. Tronconi, J. Catal. 265 (2009) 141.
[24] J.M. Fedeyko, B. Chen, H.-Y. Chen, Catal. Today, in press, ISSN 0920-5861, doi:10.1016/j.cattod.2009.12.015.
[25] J. Fedeyko, H.-Y. Chen, T. Ballinger, E. Weigert, H. Chang, J. Cox, P. Andersen, SAE 2009-01-0899.